

JOINT OPTIMIZATION OF PRIMARY AND SECONDARY TRANSFORMS USING RATE-DISTORTION OPTIMIZED TRANSFORM DESIGN

Darukeesan Pakiyarajah*, Eduardo Pavez*, Antonio Ortega*, Debargha Mukherjee†, Onur Guleryuz†, Keng-Shih Lu†, Kruthika Koratti Sivakumar†

*University of Southern California, Los Angeles, CA, USA

†Google LLC, Mountain View, CA, USA

ABSTRACT

Data-dependent transforms are increasingly being incorporated into next-generation video coding systems such as AV1, a codec under development by the Alliance for Open Media (AOM), and VVC. To circumvent the computational complexities associated with implementing non-separable data-dependent transforms, combinations of separable primary transforms and non-separable secondary transforms have been studied and integrated into video coding standards. These codecs often utilize rate-distortion optimized transforms (RDOT) to ensure that the new transforms complement existing transforms like the DCT and the ADST. In this work, we propose an optimization framework for jointly designing primary and secondary transforms from data through a rate-distortion optimized clustering. Primary transforms are assumed to follow a path-graph model, while secondary transforms are non-separable. We empirically evaluate our proposed approach using AV1 residual data and demonstrate that 1) the joint clustering method achieves lower total RD cost in the RDOT design framework, and 2) jointly optimized separable path-graph transforms (SPGT) provide better coding efficiency compared to separable KLTs obtained from the same data.

Index Terms— data-dependant primary transforms, secondary transforms, joint optimization, rate-distortion optimized transforms, separable path graph transforms

1. INTRODUCTION

Using data-dependent transforms for image and video coding has been a topic of extensive research [1–4]. Although the non-separable Karhunen-Loeve Transform (KLT) is theoretically optimal for image and residual blocks under various assumptions [5], its practical adoption is limited due to memory constraints and higher computational complexity compared to trigonometric transforms, such as the DCT, which benefit from fast implementations. To address the limitations of KLT, several alternative approaches have been proposed, including separable KLTs [1, 2], graph-based separable transforms (GBST) [6], and secondary transforms [7–13]. These methods aim to balance coding efficiency with computational complexity. Secondary transforms have been successfully integrated into VVC [14], while GBSTs and separable KLTs are being considered for next-generation codecs [14, 15]. Separable primary transforms, such as separable KLTs and GBSTs, are designed to be applied independently to the rows and columns of data blocks. On the other hand, secondary transforms are generally non-separable and are applied to a smaller subset of low-frequency primary transform coefficients

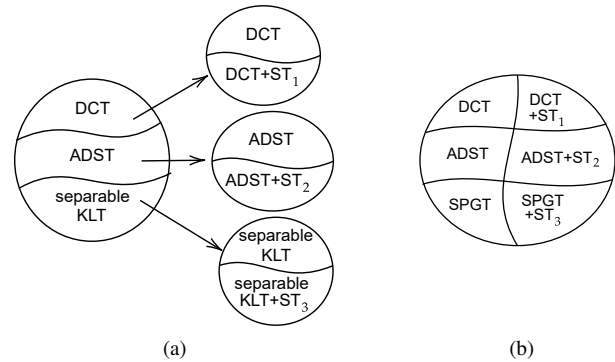


Fig. 1. Example of clustering data in an RDOT design with two three primary transforms and three secondary transforms (ST): (a) Tree-structured clustering and (b) Joint clustering with separable path graph transform (SPGT).

to refine the coding efficiency. These systems typically use a rate-distortion optimized transform (RDOT) design approach [16–18], which aims to create data-dependent transforms that minimize rate-distortion costs by using a clustering step to identify training data examples that cannot be well represented by the fixed transforms in the codec (e.g., DCT and ADST).

Current mode-dependent RDOTs for intra-prediction residuals have two major limitations. First, they are based on *independently designed primary and secondary transforms*. As shown in Fig. 1a, given the data, RDOT design and clustering are used to obtain a separable KLT and three clusters (corresponding to blocks using DCT, ADST, and the separable KLT). Subsequently, three independent RDOT design steps are performed for each cluster to design secondary transforms (ST_1 , ST_2 , and ST_3). In this tree-structured clustering, the primary transform is fixed, and the corresponding secondary transform design restricts the data in each cluster to either use a secondary transform or not, leading to a suboptimal design where the set of all primary and secondary transforms in the system may not effectively complement each other. A second limitation is that these RDOT design frameworks typically use *separable KLTs as primary transforms*, requiring the learning of $N^2/2$ parameters from the data to construct an $N \times N$ transform matrix [1, 17]. Data can be scarce for learning a specific mode-dependent transform because some intra-prediction modes are infrequently used and, if multiple transforms are learned, available residual data needs to be further split into clusters [1, 16]. Consequently, the performance of learned separable KLTs may be limited due to insufficient training data.

We address these limitations by (1) proposing a *joint rate-*

This work was supported in part by a grant from Google.

distortion optimized clustering approach to learn primary and secondary transforms and (2) employing learned *separable path graph transforms (SPGT)* as primary transforms. We are unaware of other work considering joint primary and secondary transform design and leveraging path-graph models for mode-dependent RDOT design.

In our joint design framework, all the data is clustered directly into six groups, allowing each data block to select the best combination of primary and secondary transforms from all choices in the system (see Fig. 1b). The rate-distortion-optimized primary and secondary transforms are designed simultaneously, producing clusters different from existing tree-structured clustering systems, resulting in distinct data-dependent transforms. This unified framework ensures that combinations of primary and secondary transforms are optimized to complement each other, improving data representation efficiency. Furthermore, graph-based transform learning methods have recently been shown to have advantages over traditional KLT-based methods due to their robustness and ability to learn transforms from limited data [19]. We refer readers to the works in [6, 20] for a comprehensive review of graph-based transform designs applied to image and video coding. Moreover, for path graphs, direct learning of transform parameters from data can be performed without requiring covariance matrix estimation [21]. Additionally, the path-graph model choice reduces the number of parameters learned from data to N to design transforms for rows or columns with N pixels, compared to $N^2/2$ in KLT-based methods. We leverage this in our joint learning framework to learn the SPGTs as primary transforms and address data scarcity challenges.

In designing secondary transforms, we aim to create data-dependent transforms for transform coefficients, which differ from the residual data used in primary transform design. The data scarcity problem remains a challenge and finding a suitable prior model for transform domain data is not as straightforward as in the case of rows/columns from residual data. To address the data scarcity problem, we follow previous works [7–13], which select as a secondary transform a non-separable KLT that applies to the first $n \ll N^2$ low-frequency coefficients produced by the primary transform. Furthermore, we observed that the covariance matrices of the primary transform coefficients are sparse, owing to the decorrelating effect of the primary transform. This sparsity further reduces the number of parameters and allows the corresponding KLTs to be learned from a smaller amount of data compared to the primary transforms. Thus, while non-separable KLTs would not be practical as primary transforms (2048 to be learned for 8×8 blocks), we use a non-separable KLT as a secondary transform with n small enough to make learning the parameters possible with limited amounts of data. For example, if $n = 16$, fewer than 128 parameters need to be learned due to the sparse structure of the covariance matrix. To the best of our knowledge, non-separable KLTs are always used in practice as the secondary transform [14, 22].

We empirically evaluate our proposed design of mode-dependent primary and secondary transforms using intra-prediction residual data from AV1, a codec under development by the Alliance for Open Media (AOM). Our results demonstrate that the joint clustering approach with SPGTs achieves the lowest RD cost in transform design, outperforming existing tree-structured clustering methods with separable KLTs and providing an average bitrate saving of 0.3% compared to tree-structured clustering, all without introducing additional implementation complexity. Furthermore, SPGTs achieve bitrate savings ranging from 0.5% to 3.83% over KLT-based primary transform designs, highlighting their effectiveness in learning primary transforms from limited data.

Algorithm 1 RDOT Learning

Input: $\{\mathbf{X}_i\}_{i=1}^M, \mathcal{C}_j$ for $j = 1, \dots, K$
Initialize: $\{\mathcal{S}_j\}_{j=1}^K, \{\mathbf{F}_j\}_{j=1}^K$
1: **repeat**
2: update $\mathbf{F}_j \in \mathcal{C}_j$ for $j = 1, \dots, K$
3: $\mathcal{S}_j = \left\{ i : \arg \min_k d(\mathbf{X}_i, \mathbf{F}_k) + \lambda B_{i,k} = j \right\}$
 for $j = 1, \dots, K$
4: **until** convergence
Output: $\{\mathbf{F}_j\}_{j=1}^K$

2. RATE-DISTORTION OPTIMIZED TRANSFORMS

Assume we have M residual blocks of dimension $N \times N$, $\{\mathbf{X}_i\}_{i=1}^M$, and K transforms, $\{\mathbf{F}_j\}_{j=1}^K$. Let $\tilde{\mathbf{X}}_{i,j}$ denote the transform coefficients after applying the transform \mathbf{F}_j and $d(\mathbf{X}_i, \mathbf{F}_j)$ represent the distortion due to entrywise quantization of $\tilde{\mathbf{X}}_{i,j}$. Furthermore, let $B_{i,j}$ denote the number of bits required to encode $\tilde{\mathbf{X}}_{i,j}$, including both overhead and coefficient bits. In the rate-distortion (RD) optimization step of the residual coding process, the transform \mathbf{F}_j that minimizes an RD cost is selected for each block \mathbf{X}_i . Let \mathcal{S}_j denote the index set of residual blocks that choose the transform \mathbf{F}_j :

$$\mathcal{S}_j = \left\{ i : \arg \min_k d(\mathbf{X}_i, \mathbf{F}_k) + \lambda B_{i,k} = j \right\}, \quad (1)$$

where $\lambda \geq 0$ is the predefined Lagrange multiplier commonly used in video codecs to control the RD trade-off [23]. The RDOT design problem aims to perform clustering and transform design simultaneously, which can be formulated as [16–18]

$$\begin{aligned} \min_{\{\mathbf{F}_j\}_{j=1}^K} & \sum_{j=1}^K \sum_{i \in \mathcal{S}_j} d(\mathbf{X}_i, \mathbf{F}_j) + \lambda B_{i,j} \\ \text{s.t. } & \mathbf{F}_j \in \mathcal{C}_j \quad \text{for } j = 1, \dots, K, \end{aligned} \quad (2)$$

where \mathcal{C}_j denotes the set of transforms; for instance, \mathcal{C}_j could be the set of separable transforms.

Algorithm 1, a Lloyd-type algorithm that has been employed in [16–18], solves (2) by iteratively alternating between two steps: (1) updating the transforms given the clusters based on the cluster-specific update rules and (2) updating the clusters given the transforms, where each residual block is reassigned to the cluster (transform) that minimizes its contribution to the overall objective. These steps are repeated until there is no significant change in the objective cost, indicating convergence. This approach has been used to design primary transforms based on separable KLTs [18] and secondary non-separable KLTs [7, 9]. In this work, we use this algorithm to simultaneously design SPGTs as primary transforms and non-separable KLTs as secondary transforms.

3. JOINT OPTIMIZATION OF PRIMARY AND SECONDARY TRANSFORMS

For a block \mathbf{X}_i , a separable transform can be defined using two orthonormal $N \times N$ transforms, a column transform \mathbf{C}_j and a row transform \mathbf{R}_j . The transform domain representation of \mathbf{X}_i is given by $\hat{\mathbf{X}}_{i,j} = \mathbf{C}_j^\top \mathbf{X}_i \mathbf{R}_j$. Let $\mathbf{x}_i = \text{vec}(\mathbf{X}_i)$ represent the vector formed by stacking the columns of the matrix \mathbf{X}_i . Then, the transform domain vector can be expressed as:

$$\hat{\mathbf{x}}_{i,j} = \text{vec}(\hat{\mathbf{X}}_{i,j}) = \mathbf{G}_j^\top \mathbf{x}_i, \quad (3)$$

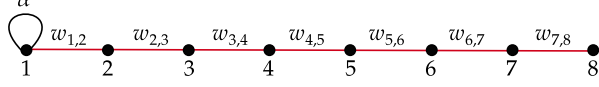


Fig. 2. A path graph model with $N = 8$ nodes, self-loop with weight α and edge weights $w_{i,j}$.

where $\mathbf{G}_j = \mathbf{R}_j \otimes \mathbf{C}_j$ denotes the separable primary transform, and \otimes denotes the Kronecker product operation on two matrices. Let \mathbf{P}_j represent the $N^2 \times N^2$ permutation matrix that reorders the elements of $\hat{\mathbf{x}}_{i,j}$ according to a scanning order (e.g., zig-zag scanning order). Suppose a non-separable orthonormal secondary transform, denoted by an $n \times n$ matrix $\tilde{\mathbf{T}}_j$, is applied to the first n low-frequency coefficients after reordering. Then, the transform coefficients obtained by applying the separable primary transform followed by the non-separable secondary transform are given by $\hat{\mathbf{y}}_{i,j} = \mathbf{T}_j^\top \mathbf{P}_j^\top \mathbf{G}_j^\top \mathbf{x}_i$, where $\mathbf{T}_j \in \mathcal{T}$ is an $N^2 \times N^2$ block matrix, and

$$\mathcal{T} = \left\{ \mathbf{T} : \mathbf{T} = \begin{bmatrix} \tilde{\mathbf{T}} & \mathbf{0} \\ \mathbf{0} & \mathbf{I} \end{bmatrix}, \tilde{\mathbf{T}}^\top \tilde{\mathbf{T}} = \mathbf{I} \right\}. \quad (4)$$

The inverse transform is $\mathbf{x} = \mathbf{F}_j \hat{\mathbf{y}}_{i,j}$, where $\mathbf{F}_j = \mathbf{G}_j \mathbf{P}_j \mathbf{T}_j$.

After entrywise quantization of $\hat{\mathbf{y}}_{i,j}$, we get $\hat{\mathbf{y}}_{i,j}^Q$. Then, the distortion of the block due to quantization is expressed as $d(\mathbf{x}_i, \mathbf{F}_j) = \|\mathbf{x}_i - \mathbf{F}_j \hat{\mathbf{y}}_{i,j}^Q\|_2^2$. During the entropy coding process with coders such as CABAC [24], $B_{i,j}$ is highly context-dependent, making it difficult to determine an accurate proxy for $B_{i,j}$ and adding complexity to the RD optimized clustering problem. To address this challenge, in [16, 17], the authors proposed using the ℓ_0 -norm of the quantized coefficients, $\|\hat{\mathbf{y}}_{i,j}^Q\|_0$, which represents the number of non-zero coefficients, as a proxy for $B_{i,j}$ in the RDOT framework. We use the same proxy in our joint learning framework, so the RD optimized clustering in step 3 of Algorithm 1 becomes:

$$\mathcal{S}_j = \left\{ i : \arg \min_k \|\mathbf{x}_i - \mathbf{F}_k \hat{\mathbf{y}}_{i,k}^Q\|_2^2 + \lambda \|\hat{\mathbf{y}}_{i,k}^Q\|_0 = j \right\}. \quad (5)$$

In our joint learning framework, we define six sets of transforms that are used for the transform updates in step 2 of Algorithm 1:

$$\begin{aligned} \mathcal{C}_1 &= \{ \mathbf{F} : \mathbf{F} = \mathbf{G}_{\text{DCT}}, \mathbf{G}_{\text{DCT}} = \mathbf{R}_{\text{DCT}} \otimes \mathbf{C}_{\text{DCT}} \}, \\ \mathcal{C}_2 &= \{ \mathbf{F} : \mathbf{F} = \mathbf{G}_{\text{ADST}}, \mathbf{G}_{\text{ADST}} = \mathbf{R}_{\text{ADST}} \otimes \mathbf{C}_{\text{ADST}} \}, \\ \mathcal{C}_3 &= \left\{ \mathbf{F} : \mathbf{F} = \mathbf{G}_{\text{SPGT}} = \mathbf{R}_3 \otimes \mathbf{C}_3, \mathbf{R}_3^\top \mathbf{R}_3 = \mathbf{C}_3^\top \mathbf{C}_3 = \mathbf{I} \right\} \cap \mathcal{G}, \\ \mathcal{C}_4 &= \{ \mathbf{F} : \mathbf{F} = \mathbf{F}_1 \mathbf{P}_4 \mathbf{T}_4, \mathbf{P}_4 \text{ fixed}, \mathbf{T}_4 \in \mathcal{T} \}, \\ \mathcal{C}_5 &= \{ \mathbf{F} : \mathbf{F} = \mathbf{F}_2 \mathbf{P}_5 \mathbf{T}_5, \mathbf{P}_5 \text{ fixed}, \mathbf{T}_5 \in \mathcal{T} \}, \\ \mathcal{C}_6 &= \{ \mathbf{F} : \mathbf{F} = \mathbf{F}_3 \mathbf{P}_6 \mathbf{T}_6, \mathbf{P}_6 \text{ fixed}, \mathbf{T}_6 \in \mathcal{T} \}, \end{aligned}$$

where \mathcal{G} denotes the path graph model constraints. Thus, the primary transforms can be either DCT, ADST or a learned SPGT. The sets \mathcal{C}_1 and \mathcal{C}_2 form a primary/secondary pair, and the same for the sets $\mathcal{C}_2/\mathcal{C}_5$ and $\mathcal{C}_3/\mathcal{C}_6$. Detailed descriptions of how SPGTs and secondary transforms are learned can be found in Section 3.1 and Section 3.2, respectively.

3.1. Separable path graph transform

Let us consider the set of SPGTs, \mathcal{C}_3 , and the corresponding data cluster \mathcal{S}_3 . In this case, we learn the inverse covariances of the column and row data, \mathbf{L}_{col} and \mathbf{L}_{row} , respectively, instead of the covariance matrices as in separable KLT methods. We adopt a model based on a path graph with a self-loop at the first node for the inverse covariance matrices of the rows and columns of $\{\mathbf{X}_i\}_{i \in \mathcal{S}_3}$. This

path graph model is parameterized by a self-loop weight α and edge weights $w_{i,j}$, as illustrated in Fig. 2. The choice of this path graph model is motivated by the fact that a path graph with no self-loop and all edge weights equal to 1 corresponds to DCT, while adding a self-loop with weight 1 at the first node corresponds to ADST. In [21], it has been shown that the solution of the graph learning problem in [6] is provided by closed-form formulas giving the edge weights and the self-loop weight:

$$\begin{aligned} w_{i,j} &= \left[\frac{1}{P} \sum_{p=1}^P (x_p(i) - x_p(j))^2 + \beta \right]^{-1}, \\ \alpha &= \left[\frac{1}{P} \sum_{p=1}^P x_p^2(1) \right]^{-1}, \end{aligned}$$

where P is the number of training samples used to learn the model parameters, $x_p(i)$ represents the data observed at the i^{th} node of the graph for the p^{th} training sample, and $\beta > 0$ is a small positive number to avoid infinity. Then the transforms \mathbf{C}_3 and \mathbf{R}_3 are given by the eigenbasis of \mathbf{L}_{col} and \mathbf{L}_{row} respectively, and the SPGT corresponding to this cluster is given by $\mathbf{G}_{\text{SPGT}} = \mathbf{R}_3 \otimes \mathbf{C}_3$.

Note that in this case, we obtain an $N \times N$ transform by learning only N parameters from the data, α and $w_{i,j}$, whereas the separable KLT approaches in [1, 17] need to learn $N^2/2$ parameters. This significant reduction in the number of learned parameters can be particularly beneficial in data-scarce scenarios, such as when dealing with less frequent intra-prediction modes or smaller clusters in the clustering framework, where sufficient training data is limited.

3.2. Secondary transform

Consider the case where the transform corresponding to the j^{th} cluster is a primary transform followed by a secondary transform, with \mathbf{G}_j and \mathbf{P}_j fixed a priori. This set of transforms can be expressed by

$$\mathcal{C}_j = \{ \mathbf{F} : \mathbf{F} = \mathbf{G}_j \mathbf{P}_j \mathbf{T}_j, \mathbf{G}_j, \mathbf{P}_j \text{ are fixed}, \mathbf{T}_j \in \mathcal{T} \}. \quad (6)$$

Here, \mathbf{G}_j could be any predefined separable transform. We use an empirical approach to obtain \mathbf{P}_j for each intra-prediction mode in our setting. We apply the fixed separable primary transform, \mathbf{G}_j , assigned to this cluster to $\{\mathbf{X}_i\}_{i \in \mathcal{S}_j}$. Then, we compute the sample variance of each of these transform coefficients. The sorting order of the transform coefficients based on their decreasing sample variance determines the permutation matrix \mathbf{P}_j . Then, the secondary transform is obtained by solving the following optimization [8–10]:

$$\begin{aligned} \mathbf{F}_j &= \arg \min_{\mathbf{F} \in \mathcal{C}_j} \sum_{i \in \mathcal{S}_j} \|\mathbf{x}_i - \mathbf{F} \hat{\mathbf{y}}_{i,j}^Q\|_2^2 \\ &= \mathbf{G}_j \mathbf{P}_j \left[\arg \min_{\mathbf{T}_j \in \mathcal{T}} \sum_{i \in \mathcal{S}_j} \|\hat{\mathbf{z}}_{i,j} - \mathbf{T}_j \hat{\mathbf{z}}_{i,j}^Q\|_2^2 \right], \end{aligned} \quad (7)$$

where $\hat{\mathbf{z}}_{i,j} = \mathbf{P}_j^\top \mathbf{G}_j^\top \mathbf{x}_i$, the second equality follows from the Parseval's identity. In [8–10], it has been shown that the solution \mathbf{T}_j in the above problem is obtained by first computing the non-separable secondary transform $\tilde{\mathbf{T}}_j$ as the non-separable KLT of the n significant frequency coefficients derived from all the residual data in this cluster and then, \mathbf{T}_j is constructed from $\tilde{\mathbf{T}}_j$ such that $\mathbf{T}_j \in \mathcal{T}$.

4. EMPIRICAL RESULTS

We use intra-prediction residuals obtained from AVIM for both learning and testing transforms in our experiments.

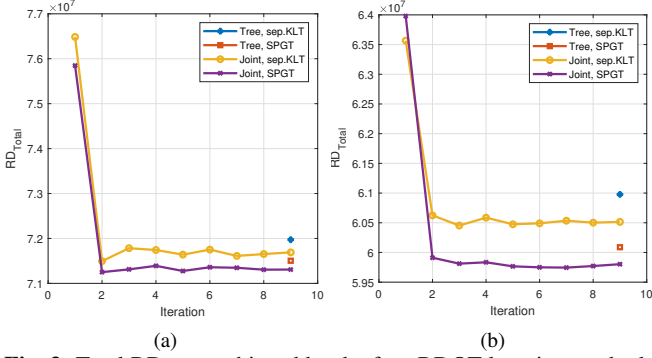


Fig. 3. Total RD cost achieved by the four RDOT learning methods for (a) H-PRED and (b) D_135_PRED. For tree-structured clustering, RD_{Total} is computed after designing all transforms and represented as points.

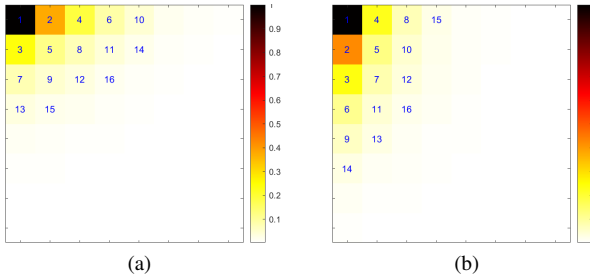


Fig. 4. Sample variance (normalized) of the transform coefficients after applying separable DCT, corresponding to intra-prediction modes: (a) V-PRED), and (b) H-PRED. The numbers 1–16 indicate the coefficients selected for the secondary transform.

4.1. Mode-dependent RDOT learning

We design data-dependent primary and secondary transforms for the 12 principal intra-prediction modes in AVM in a mode-dependent manner. In this setup, each intra-prediction mode is allowed to use six ($K = 6$) transforms, and the joint RDOT learning is performed as described in Section 3. We refer to our approach as joint clustering with SPGT (Joint, SPGT).

First, we show how the low-frequency coefficients are selected for different intra-prediction modes for the subsequent secondary transform. Examples of the sample variance of the transform coefficients obtained for two different intra-prediction modes of AVM after applying G_{DCT} as the primary transform are shown in Fig. 4. This highlights the importance of adopting a mode-dependent scanning order to select the low-frequency coefficients for the subsequent secondary transform rather than relying on a fixed order for all modes. Examples of the 16 coefficients selected for two different 8×8 intra-prediction modes of AVM are illustrated in Fig. 4.

Moreover, to compare against the existing tree-structured clustering approaches [10, 13], we design primary and secondary transforms following these steps:

1. Run Algorithm 1 with $\{\mathbf{X}_i\}_{i=1}^M$, C_1 , C_2 , and C_3 as inputs to obtain G_{SPGT} and the clusters S_1 , S_2 , and S_3 .
2. Run three independent instances of Algorithm 1 to design the secondary transforms with (i) $\{\mathbf{X}_i\}_{i \in S_1}$, C_1 , C_4 , (ii) $\{\mathbf{X}_i\}_{i \in S_2}$, C_2 , C_5 , (iii) $\{\mathbf{X}_i\}_{i \in S_3}$, C_3 , C_6 as inputs to obtain secondary transforms.

We refer to this method as tree-structured clustering with SPGT (Tree, SPGT). To compare the SPGTs against the separable KLTs method for designing primary transforms, we repeat the joint and

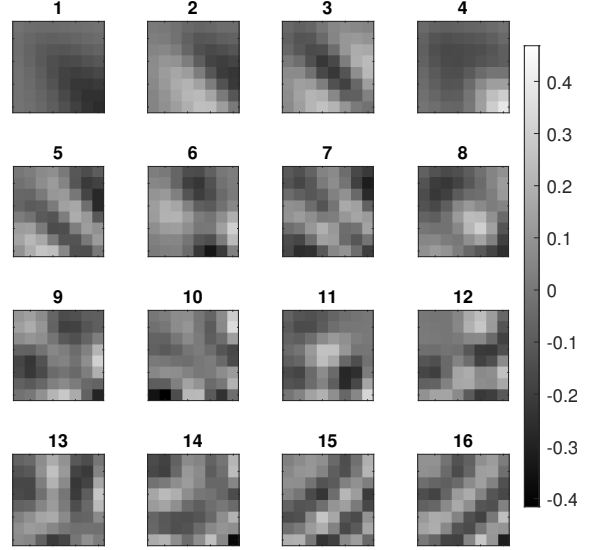


Fig. 5. First 16 columns (basis) of the transform $F_6 = G_{SPGT} P_6 T_6$ designed using the joint learning with SPGT for D_135_PRED (diagonal prediction), 8×8 residuals, reshaped into 8×8 blocks.

tree-structured clustering of the same data, but with F_3 obtained using the separable KLT method as described in [1], where the R_3 and C_3 are obtained from the eigenbasis of S_{col} and S_{row} , the sample covariance matrices of rows and columns of $\{\mathbf{X}_i\}_{i \in S_3}$, respectively.

Note that we have two clustering approaches, {Joint, Tree}, and two transform learning methods to design primary transforms, {SPGT, sep.KLT}, with each combination of clustering and transform learning resulting in four methods to design RDOTs: (Joint, SPGT), (Joint, sep.KLT), (Tree, SPGT), and (Tree, sep.KLT). For our experiments, we consider training data consisting of 8×8 and 16×16 residuals and train mode-dependent transforms separately for each block size. The number of coefficients selected for secondary transforms is set to $n = 16$ for 8×8 blocks and $n = 64$ for 16×16 blocks. Furthermore, in RDOT design, we use $QP = 28$ and $\lambda = 0.85 \times 2^{(QP-12)/3}$, which are typical values used for RDOT design for intra-prediction residuals in codecs like AVC and HEVC [17, 18]. In our experiments with different values of QP (or λ), we observed that training the transforms with a smaller QP (smaller λ) from the typical range of QP values used in compression applications allows the same transforms to be used across different QP values. This eliminates the need to train transforms for different QP values without a significant trade-off in bitrate savings. Furthermore, for each cluster corresponding to the secondary transforms, we observed that the covariance matrices of the n low-frequency transform coefficients are of full rank, substantiating that non-separable KLTs with fewer parameters can effectively learn the secondary transforms. We omit the detailed experimental results due to space limitations.

The first 16 basis functions of the transform $F_6 = G_{SPGT} P_6 T_6$ designed using the joint learning method for D_135_PRED (diagonal prediction), 8×8 residuals are shown in Fig. 5. From the figure, we observe that the low-frequency basis functions exhibit smooth variations in the direction of the corresponding intra-prediction mode, demonstrating that the combination of primary and secondary transforms effectively adapts to the statistics of the data. Further, to compare these four learning methods, we compute the total RD cost ob-

Method	DC	V	H	D_45	D_135	D_113	D_157	D_203	D_67	S	S_V	S_H
Tree, sep. KLT	-1.54	-2.62	-2.43	-7.35	-8.36	-6.48	-5.73	-5.94	-8.09	-4.05	-3.78	-4.63
Joint, sep. KLT	-1.76	-3.17	-2.78	-7.43	-8.63	-6.90	-5.90	-6.64	-8.70	-4.48	-3.90	-4.83
Tree, SPGT	-2.65	-3.33	-4.97	-10.04	-11.28	-9.14	-9.15	-8.92	-9.64	-5.82	-5.09	-6.76
Joint, SPGT	-2.77	-4.02	-5.32	-10.30	-11.51	-9.32	-9.73	-9.48	-10.11	-6.01	-5.12	-7.00

Table 1. BD rate savings (%) with respect to the baseline for 8×8 residuals. More negative values indicate greater bitrate savings.

Method	DC	V	H	D_45	D_135	D_113	D_157	D_203	D_67	S	S_V	S_H
Tree, sep. KLT	-3.97	-1.70	-2.21	-8.44	-11.58	-9.70	-8.52	-8.34	-9.26	-4.96	-1.89	-3.90
Joint, sep. KLT	-4.07	-2.77	-2.91	-8.73	-11.86	-10.10	-8.79	-8.57	-9.44	-5.22	-3.52	-4.41
Tree, SPGT	-4.36	-3.29	-3.88	-9.56	-13.18	-10.67	-9.89	-9.62	-10.47	-5.66	-3.85	-5.60
Joint, SPGT	-4.57	-3.96	-4.16	-9.77	-13.50	-10.85	-9.98	-9.73	-10.73	-5.94	-4.78	-5.93

Table 2. BD rate savings (%) with respect to the baseline for 16×16 residuals. More negative values indicate greater bitrate savings.

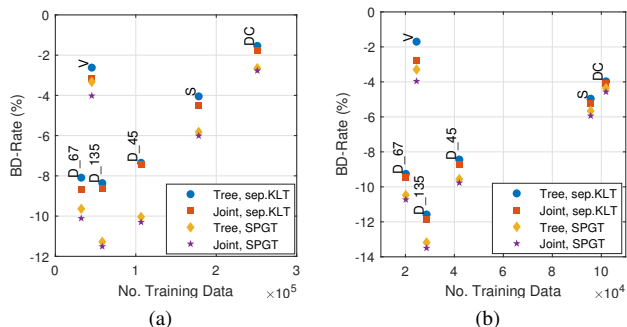


Fig. 6. BD-rate saving vs the number of data samples used to train RDOTs for (%) (a) 8×8 residual blocks and (b) 16×16 residual blocks. The points along the same vertical line correspond to the same (labeled) intra-prediction mode, with more negative values indicating greater bitrate savings.

tained using these methods, given by

$$\text{RD}_{\text{Total}} = \sum_{j=1}^K \sum_{i \in S_j} \|\mathbf{x}_i - \mathbf{F}_j \hat{\mathbf{y}}_{i,j}^Q\|_2^2 + \lambda \|\hat{\mathbf{y}}_{i,j}^Q\|_0, \quad (8)$$

for 8×8 intra-prediction residuals corresponding to all the intra-prediction modes. The results for two of those modes are presented in Fig. 3. From this figure, we observe the following: 1) both joint clustering methods achieve a lower total RD cost compared to their respective tree-structured clustering methods, and 2) methods employing SPGTs achieve a lower objective cost compared to those using separable KLTs. These observations are consistent across all intra-prediction modes and provide empirical evidence supporting our claims regarding the benefits of joint clustering and the advantages of path graph-based transforms.

4.2. Testing

Next, we demonstrate that the transforms designed using the joint clustering method with SPGT provide better coding gains than other methods in video coding applications. For this purpose, we use a different test dataset of residuals from AVM. For each intra-prediction mode, we independently encode each residual block. The process involves applying the transform, uniform quantization of transform coefficients with quantization parameters $QP = \{26, 27, 28, 29, 30, 31\}$, and entropy coding the coefficients using a CAVLC encoder [25]. We first select the best primary transform from the three primary transforms for each block through a standard RDO process. Then, we perform a secondary RDO step to decide whether or not to apply a secondary transform. We use a fixed

3-bit overhead to signal the selected transform for each block: two bits to indicate the primary transform and one bit to signal whether a secondary transform is applied. This RDO approach for choosing the best combination of primary and secondary transforms is consistent with state-of-the-art codecs using secondary transforms.

We compare all four learning methods against a baseline method that uses only two primary transforms, DCT and ADST, with RDO, quantization, and entropy coding performed as described. The baseline has only two primary transforms and uses only a one-bit overhead to signal the selected transform. For each method, including the baseline, we compute the bitrate and distortion for each block and average the results across multiple blocks. We present the average Bjontegaard rate (BD-rate) savings [26] compared to the baseline for each intra-prediction mode of 8×8 blocks in Table 1 and 16×16 blocks in Table 2. Note that since all transform learning is performed offline, the bitrate reductions come at no additional implementation cost. Furthermore, most of the gain in the transform design is achieved by using SPGTs. Significant gains in directional prediction modes suggest that data-dependent transforms effectively adapt to their directional statistics. An average of 0.3% bitrate reduction from the joint clustering compared to tree-structured clustering indicates that the primary and secondary transforms are better optimized to complement each other compared to tree-structured clustering. Furthermore, we present the BD-rate savings for all methods as a function of the number of data samples used to train the RDOTs in Fig. 6a and Fig. 6b. For modes with fewer training samples, the difference between KLT-based methods and SPGTs is significant, while the difference diminishes for modes with larger amounts of training data. This highlights the advantage of using path graph prior to learn transforms with fewer parameters in data-scarce scenarios.

5. CONCLUSION

In this work, we proposed a method for simultaneously learning data-dependent primary and secondary transforms using the rate-distortion optimized transform design framework. To learn the separable primary transforms, we utilized a path graph model with a self-loop at the first node, enabling efficient transform learning with fewer parameters in data-scarce scenarios. We empirically evaluated our approach using AVM intra-prediction residuals, comparing joint versus tree-structured clustering and separable KLTs versus SPGTs for transform learning. Our experimental results demonstrated that SPGTs offer significant gains over KLT-based methods in data-limited scenarios, and joint clustering produces more efficient transforms than tree-structured clustering. Future work will focus on implementing and evaluating the proposed joint transform design approach within state-of-the-art video codecs.

6. REFERENCES

- [1] Chuohao Yeo, Yih Han Tan, Zhengguo Li, and Susanto Rahardja, "Mode-dependent transforms for coding directional intra prediction residuals," *IEEE Transactions on Circuits and Systems for Video Technology*, vol. 22, no. 4, pp. 545–554, 2012.
- [2] Kui Fan, Ronggang Wang, Weisi Lin, Ling-Yu Duan, and Wen Gao, "Signal-independent separable KLT by offline training for video coding," *IEEE Access*, vol. 7, pp. 33087–33093, 2019.
- [3] Long Xu, King Ngi Ngan, and Miaohui Wang, "Video content dependent directional transform for intra frame coding," in *2012 Picture Coding Symposium*. IEEE, 2012, pp. 197–200.
- [4] Adrià Arrufat, Pierrick Philippe, and Oliver Déforges, "Non-separable mode dependent transforms for intra coding in HEVC," in *2014 IEEE Visual Communications and Image Processing Conference*. IEEE, 2014, pp. 61–64.
- [5] Shuyuan Zhu and Bing Zeng, "A comparative study of image correlation models for directional two-dimensional sources," in *2011 IEEE 13th International Workshop on Multimedia Signal Processing*, 2011, pp. 1–5.
- [6] Hilmi E. Egilmez, Yung-Hsuan Chao, Antonio Ortega, Bumshik Lee, and Sehoon Yea, "GBST: Separable transforms based on line graphs for predictive video coding," in *2016 IEEE International Conference on Image Processing (ICIP)*, 2016, pp. 2375–2379.
- [7] Amir Said, Xin Zhao, Marta Karczewicz, Hilmi E. Egilmez, Vadim Seregin, and Jianle Chen, "Highly efficient non-separable transforms for next-generation video coding," in *2016 Picture Coding Symposium (PCS)*, 2016, pp. 1–5.
- [8] Xin Zhao, Li Li, Zhu Li, Xiang Li, and Shan Liu, "Coupled primary and secondary transform for next generation video coding," in *2018 IEEE Visual Communications and Image Processing (VCIP)*, 2018, pp. 1–4.
- [9] Xin Zhao, Jianle Chen, Marta Karczewicz, Amir Said, and Vadim Seregin, "Joint separable and non-separable transforms for next-generation video coding," *IEEE Transactions on Image Processing*, vol. 27, no. 5, pp. 2514–2525, 2018.
- [10] Xin Zhao, Jianle Chen, Amir Said, Vadim Seregin, Hilmi E. Egilmez, and Marta Karczewicz, "NSST: Non-separable secondary transforms for next generation video coding," in *2016 Picture Coding Symposium (PCS)*, 2016, pp. 1–5.
- [11] Moonmo Koo, Mehdi Salehifar, Jaehyun Lim, and Seung-Hwan Kim, "Low frequency non-separable transform (LFNST)," in *2019 Picture Coding Symposium (PCS)*, 2019, pp. 1–5.
- [12] Ankur Saxena and Felix C. Fernandes, "On secondary transforms for intra prediction residual," in *2012 IEEE International Conference on Acoustics, Speech and Signal Processing (ICASSP)*, 2012, pp. 1201–1204.
- [13] Xin Zhao and Shan Liu, "Unified secondary transform for intra coding beyond AV1," in *2020 IEEE International Conference on Image Processing (ICIP)*, 2020, pp. 3393–3397.
- [14] Xin Zhao, Liang Zhao, Madhu Krishnan, Yixin Du, Shan Liu, Debargha Mukherjee, Yaowu Xu, and Adrian Grange, "Study on coding tools beyond AV1," in *2021 IEEE International Conference on Multimedia and Expo (ICME)*. IEEE, 2021, pp. 1–6.
- [15] Hilmi Enes Egilmez, Amir Said, Vadim Seregin, and Marta Karczewicz, "Parametric graph-based separable transforms for video coding," Aug. 30 2022, US Patent 11,432,014.
- [16] Feng Zou, Oscar C. Au, Chao Pang, Jingjing Dai, Xingyu Zhang, and Lu Fang, "Rate-distortion optimized transforms based on the Lloyd-type algorithm for intra block coding," *IEEE Journal of Selected Topics in Signal Processing*, vol. 7, no. 6, pp. 1072–1083, 2013.
- [17] Xin Zhao, Li Zhang, Siwei Ma, and Wen Gao, "Video coding with rate-distortion optimized transform," *IEEE Transactions on Circuits and Systems for Video Technology*, vol. 22, no. 1, pp. 138–151, 2012.
- [18] Adrià Arrufat, Pierrick Philippe, and Oliver Déforges, "Rate-distortion optimised transform competition for intra coding in HEVC," in *2014 IEEE Visual Communications and Image Processing Conference*, 2014, pp. 73–76.
- [19] Wen-Yang Lu, Eduardo Pavez, Antonio Ortega, Xin Zhao, and Shan Liu, "Online-learned graph transforms for adaptive block size intra-predictive coding," in *Applications of Digital Image Processing XLVII*. SPIE, 2024, vol. 13137, pp. 443–450.
- [20] Eduardo Pavez, Antonio Ortega, and Debargha Mukherjee, "Learning separable transforms by inverse covariance estimation," in *2017 IEEE International Conference on Image Processing (ICIP)*. IEEE, 2017, pp. 285–289.
- [21] Keng-Shih Lu and Antonio Ortega, "Closed form solutions of combinatorial graph Laplacian estimation under acyclic topology constraints," *arXiv preprint arXiv:1711.00213*, 2017.
- [22] Benjamin Bross, Ye-Kui Wang, Yan Ye, Shan Liu, Jianle Chen, Gary J Sullivan, and Jens-Rainer Ohm, "Overview of the versatile video coding (VVC) standard and its applications," *IEEE Transactions on Circuits and Systems for Video Technology*, vol. 31, no. 10, pp. 3736–3764, 2021.
- [23] Daniel Joseph Ringis, Vibhoothi, François Pitié, and Anil Kokaram, "The disparity between optimal and practical Lagrangian multiplier estimation in video encoders," *Frontiers in Signal Processing*, vol. 3, pp. 1205104, 2023.
- [24] D. Marpe, G. Blattermann, G. Heising, and T. Wiegand, "Video compression using context-based adaptive arithmetic coding," in *Proceedings 2001 International Conference on Image Processing (Cat. No.01CH37205)*, 2001, vol. 3, pp. 558–561 vol.3.
- [25] Marta Karczewicz and Justin Ridge, "Context-based adaptive variable length coding for adaptive block transforms," Sept. 21 2004, US Patent 6,795,584.
- [26] G Bjontegaard, "Calculation of average PSNR differences between RD-curves," *ITU-T SG16 Q*, vol. 6, 2001.